Front. Earth Sci. 2022, 16(4): 1052−1060
https://doi.org/10.1007/s11707-022-0982-5

RESEARCH ARTICLE

Impacts of cloud radiative processes on the convective and stratiform rainfall associated with Typhoon Fitow (2013)

Huiyan XU, Dengrong ZHANG (✉)

Zhejiang Provincial Key Laboratory of Urban Wetlands and Regional Change, Hangzhou Normal University, Hangzhou 311121, China

Abstract The three-dimensional Weather Research and Forecasting (WRF) model was used to conduct sensitivity experiments during the landfall of Typhoon Fitow (2013) to examine the impacts of cloud radiative processes on thermal balance. The vertical profiles of heat budgets, vertical velocity, and stability were analyzed to examine the physical processes responsible for cloud radiative effects on surface rainfall for Typhoon Fitow (2013). The inclusion of clouds reduced radiative cooling in ice and liquid cloud layers by reducing outgoing radiation. The suppressed radiative cooling reduced from the ice cloud layers to liquid cloud layers. This was conducive to reducing instability. The decreased instability was associated with the reduced upward motions. The reduced upward motion led to a decreased vertical mass convergence. Consequently, heat divergence was weakened to warm the atmosphere. Together with suppressed radiative cooling, these effects jointly suppressed net condensation and rainfall. Furthermore, the reduced rainfall due to the cloud radiative effects were mainly associated with the reduced convective and stratiform rainfall. The reduced convective rainfall was associated with the reduced net condensation, while the reduced stratiform rainfall was related to the constraint of hydrometeor convergence.

Keywords heat budget, radiative cooling, heat divergence, latent heat release, typhoon

1 Introduction

Cloud radiative processes have an important impact on convective clouds and associated precipitation by regulating vertical thermal stratification. They consist of both solar shortwave radiation and infrared longwave radiation. Radiative cooling may influence cloud formation (Lilly, 1988; Xu and Randall, 1995a), convection (Gray and Jacobson, 1977; Fu et al., 1995), surface rainfall (Dudhia, 1989; Xu and Randall, 1995b), relative humidity (Fu et al., 1995; Tao et al., 1996), and precipitable water (Sui et al., 1997, 1998; Gao et al., 2009; Gao and Li, 2010). Heat budget is one of the most important physical constraints in linking radiative cooling to the release of latent heat, sensible heat, and divergence of heat flux. When large-scale circulation is absent, the equilibrium modeling study shows that the release of latent heat is generally offset by radiative cooling (e.g., Li and Gao, 2011). The exclusion of cloud radiative processes of liquid or ice clouds may enhance the release of latent heat in response to strengthened radiative cooling and lead to enhanced surface rainfall. Cloud radiation effects may also affect surface rainfall by impacting hydrometeor distributions, e.g., Yin et al. (2022) improved the 24-h heavy rainfall during the period from 0000 UTC 21 to 0000 UTC 22 July 2012 in the East Asia Monsoon Region by improving raindrop and snow size distributions.

When a cloud-resolving model is imposed by large-scale forcing, Sui et al. (1994) revealed that the divergence of heat flux largely balances out latent heat release. Radiative cooling is relatively less important in the heat budget. Cloud radiative effects on heat budget show that change in radiative cooling may regulate changes in the release of latent heat and the divergence of heat flux, which then affect surface rainfall. Wang et al. (2010a, 2010b) and Shen et al. (2011a, 2011b) conducted a series of sensitivity experiments on severe tropical storm Bilis (2006) and a pre-summer torrential rainfall case over southern China, respectively. They revealed that the exclusion of cloud radiative effects barely changes the release of latent heat while the suppressed heat divergence corresponds to enhance radiative cooling, leading to increased surface rainfall. Shen et al. (2010) examined the thermodynamics of tropical precipitation processes and showed that in the case of mean water vapor

Received November 10, 2021; accepted March 3, 2022

E-mail: zju_rs@126.com

divergence, the mean heat divergence mainly balances the mean latent heat and affects surface rainfall. Wang et al. (2018) conducted sensitivity experiments on Typhoon Soudelor in 2015 to examine the responses of surface rainfall to the radiative effects of different cloud species and showed that different cloud species affect precipitation through different cloud radiation feedback mechanisms. As a result, the inclusion of radiative effects of cloud ice reduced vertical mass divergence and the divergence of heat flux due to reduced net condensation and rainfall, and vice versa when including radiative effects of snow (Wang et al., 2018). Zhu et al. (2018) investigated the thermal and microphysical effects of ice clouds on rainfall by examining heat budgets of a torrential rainfall simulation in north China in July 2013 and showed that the radiative feedback of ice clouds during the day is different from that at night. Their results showed that the inclusion of latent heat effects of ice clouds suppressed instability and updrafts during nighttime as a result of constraint surface rainfall, while the inclusion of radiative effects of ice clouds enhanced instability and updrafts in the early morning as a result of increased surface rainfall. Precipitation systems are decomposed into convective and stratiform rainfall to better understand convection-generated rainfall. Convective and stratiform rainfall are different in their vertical velocity distributions, microphysical processes, and rainfall characteristics. Steiner and Houze (1993) and Houze (1997) show that stratiform rainfall generally has weak horizontal gradients and/or a bright band, and vertical air motions are generally stronger in convective rainfall regions than in non-convective rainfall regions. Other studies show that the collection of cloud water and vapor deposition are dominant in convective rainfall and stratiform rainfall (Houze, 1997; Sui et al., 2007; Li et al., 2014; Shu et al., 2020). Convective rainfall is dominant in the hydrological cycle since it is usually strong, while stratiform rainfall is important in cloud radiation budgets since it is widespread with large cloud coverage (Feng et al., 2011). Understanding the cloud radiation effects on convective and stratiform rainfall may be favorable to accurately predict the convective rainfall intensity and the rainfall coverage of stratiform rainfall, which has potential effects on improving rainfall prediction. Cloud radiative processes may affect rainfall as well as convective and stratiform rainfall through changing atmospheric stratification. Motivated by the potentially different effects of cloud radiation on convective and stratiform rainfall, this paper will first investigate the effects of cloud radiation on rainfall and then analyze the effects of cloud radiation on convective and stratiform rainfall. Unlike cloud-resolving models imposed by large-scale forcing, the Weather Research and Forecasting (WRF) model allows the interaction between clouds and environmental circulations.

This study used the WRF model to conduct a pair of sensitivity experiments on Typhoon Fitow (2013) during its landfall. The model and experimental designs are briefly described in Section 2. The impacts of cloud radiative processes on thermal balance are analyzed in Section 3. Section 4 gives a summary.

2 Model and experiment design

At its peak, Typhoon Fitow formed on September 30, 2013, over the eastern Philippines, strengthened to a typhoon around 2100 UTC on October 2 and made landfall with a minimum pressure of 955 hPa and a maximum wind speed of 42 $m \cdot s^{-1}$ in Fuding, Fujian at 1715 UTC on October 7 (see a detailed overview in Yu (2014)).

In this study, the Weather Research and Forecasting model of version 3.5.1 (WRFV3.5.1) is employed to investigate the impacts of cloud radiative processes on the thermal balance associated with typhoon Fitow (2013). Three model domains with two-way nesting are used with horizontal grid resolutions of 27, 9, and 3 km and dimensions of 174 × 120 in the west-east and south-north directions for domain 1 (d01), 211 × 196 for domain 2 (d02), and 361 × 223 for domain 3 (d03) (see Fig. 1(a) in Xu and Li (2017)). The WRF model setups are summarized in Table 1. The control experiment has been validated with available observations in terms of typhoon track, minimum sea level pressure, surface precipitation, radar reflectivity, and vertical profiles of temperature, specific humidity, and winds (Xu and Li, 2017). In addition to the control experiment, another sensitivity experiments was conducted to examine the cloud radiative effects on thermal balance. The sensitivity experiment is identical to the control experiment except that the cloud hydrometeor mixing ratios in the calculations of both solar and infrared radiative processes are set to zero.

For typhoon cases, the commonly used methods to partition convective or stratiform rainfall are based on surface rainfall (Braun et al., 2010). Braun et al. (2010) (hereafter Braun10) identified convective rainfall at grid points where surface rain rates are over 20 mm/h, or at least twice as large as the mean value of their nearest 24 neighbors. The air columns with a vertical velocity greater than 3 m/s or liquid cloud water greater than 0.5 g/kg are also identified as convective rainfall. The remaining grid points are considered stratiform, where the surface rain rate is over 0.1 mm/h. More details about the Braun10 convective-stratiform rainfall partition scheme can be referred to Braun et al. (2010).

3 Results

The surface rainfall equation and heat budget are first analyzed to examine cloud radiative effects on surface

Table 1 WRF Model setup

Vertical levels	33
Model top	50 hPa
Shortwave radiation scheme	Dudhia (1989)
Longwave radiation scheme	Mlawer et al. (1997)
Cloud microphysical scheme	Lin et al. (1983)
Land surface scheme	Dudhia (1996)
Cumulus scheme	N/A
Data used for initial and lateral boundary conditions	National Centers for Environmental Prediction (NCEP) global forecast system (GFS) final (FNL) operational global analysis
Model integration period	0000 UTC 6 October – 1200 UTC 7 October 2013
Data analysis period	1200 UTC 6 October – 1200 UTC 7 October 2013

rainfall. Following Skamarock et al. (2008), Xu and Li (2017), and Wang et al. (2018), the surface rainfall budget in the 3D WRF model framework can be written as

$$P_S = Q_{NC} + Q_{CM}, \tag{1}$$

where P_S is the rain rate, Q_{NC} is net condensation, and Q_{CM} is cloud hydrometeor convergence/divergence.

The inclusion of radiative effects from clouds reduce surface rainfall from NCR to CTL. The decrease in rainfall in the CTL experiment is primarily due to decreased net condensation (Table 2).

To explain the responses of surface rainfall to the cloud radiative processes, the heat budget is analyzed. Following Skamarock et al. (2008), the heat budget can be written as

$$F_{loc} = F_{hd} + F_{rad} + F_{pbl} + F_{mp}, \tag{2}$$

where

$$F_{loc} = \frac{\partial T}{\partial t}, \tag{2.1}$$

$$F_{hd} = \pi[-(\nabla \cdot \vec{V}\theta)], \tag{2.2}$$

$$F_{rad} = \pi F_{rad*} \tag{2.3}$$

$$F_{pbl} = \pi F_{pbl*} \tag{2.4}$$

$$F_{mp} = \pi F_{mp*} \tag{2.5}$$

where T and θ are air temperature and potential temperature, respectively; $\vec{V}$ is a three-dimensional wind vector $\pi = (p/p_o)^{\kappa}$, p_o = 1000 hPa, $\kappa = R/c_p$, R is the gas constant, c_p is the specific heat of dry air at constant pressure and F_{rad*} is the tendency term due to radiation. F_{pbl*} is sensible heat, and F_{mp*} is latent heat. Eq. (1) states that temperature tendency (F_{loc}) is associated with the divergence of heat flux (F_{hd}), solar and infrared radiative processes (F_{rad}), sensible heat (F_{pbl}), and the release of latent heat (F_{mp}). Some terms, including diffusion and Rayleigh damping, are not included in Eq. (1) because they are negligibly small.

Table 2 Daily and model domain means of surface rain rate (P_S), net condensation (Q_{NC}), and hydrometeor convergence/divergence (Q_{CM}) for surface rainfall in CTL, and NCR, and their differences (CTL−NCR)

	CTL	NCR	CTL−NCR
P_S	69.550	72.710	−3.160
Q_{NC}	69.710	73.630	−3.920
Q_{CM}	−0.170	−0.890	0.720

The comparison of heat budgets between CTL and NCR (Fig. 1) reveals that cloud radiative processes reduce the radiative cooling effects in the troposphere (below 11 km). The decreased net condensation (Table 2) is mainly related to the constraint release of latent heat. The weakened release of latent heat is due to the reduced radiative cooling and the suppressed heat flux divergence.

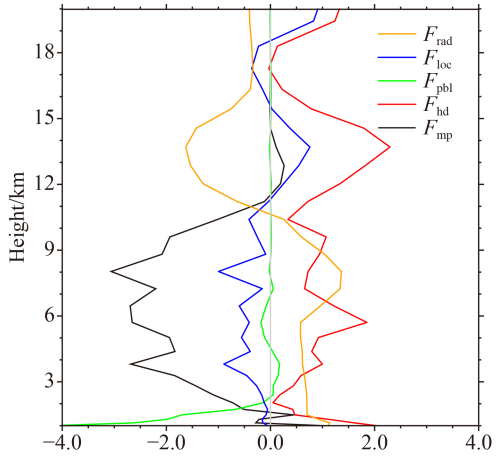

Fig. 1 Vertical profiles of differences in temperature tendency (F_{loc}; blue) and its tendency due to heat divergence (F_{hd}; red), sensible heat (F_{pbl}; green), latent heat (F_{mp}; black) and radiative processes (F_{rad}; orange) between the control experiment and the sensitivity experiment. Unit is °C·d^{-1}.

The above analysis indicates that the change in latent heat release corresponds to the change in the heat flux divergence from NCR to CTL. Thus, the change in the divergence of heat flux is further analyzed. The heat flux divergence ($F_{\rm hd}$) can be decomposed to two components:

$$F_{\rm hd} = xytend + ztend. \tag{3}$$

The heat flux divergence ($F_{\rm hd}$) can be decomposed to the horizontal (*xytend*) and vertical (*ztend*) heat flux divergence.

Figure 2 reveals that the decrease in the heat flux divergence from the sensitivity experiment to the control experiment is associated with the decrease in the vertical heat fluxdivergence. Thus, the decrease in the suppression of divergence in vertical heat flux corresponds to the decrease in radiative cooling. Overall, the suppressed divergence of vertical heat flux is primarily responsible for the weakened divergence of heat flux from NCR to CTL below 11 km (Fig. 2).

The vertical heat flux divergence can be decomposed to

$$ztend = -\overline{\frac{\pi}{\mu}\frac{\partial \omega\theta}{\partial\sigma}} = ztend1 + ztend2 + ztend3, \tag{4}$$

$$ztend1 = -\frac{\overline{\pi}}{\mu}\overline{\omega}\frac{\partial\overline{\theta}}{\partial\sigma}, \tag{4.1}$$

$$ztend2 = -\frac{\overline{\pi}}{\mu}\overline{\theta}\frac{\partial\overline{\omega}}{\partial\sigma}, \tag{4.2}$$

$$ztend3 = -\overline{\frac{\pi}{\mu}\frac{\partial\omega'\theta'}{\partial\sigma}}. \tag{4.3}$$

where ω is the vertical velocity in p-coordinate, overbar denotes domain mean, *ztend*1, *ztend*2, and *ztend*3 are mean vertical temperature advection, the interaction between mean temperature and vertical divergence, and the divergence of perturbation vertical heat flux, respectively.

Figure 3 shows that the reduction in *ztend* is related to the decrease in *ztend*2. As a result, a reduction in interaction between mean vertical divergence and mean temperature correlates with the reduction in radiative cooling.

*ztend*2 can be further expressed as

$$ztend2 = F_\theta F_{d\omega}, \tag{5}$$

where

$$F_\theta = \overline{\theta}, \tag{5.1}$$

$$F_{d\omega} = -\frac{\overline{\pi}}{\mu}\frac{\partial\overline{\omega}}{\partial\sigma}, \tag{5.2}$$

F_θ is mean temperature, and $F_{d\omega}$ is mean vertical divergence.

Figure 3 further shows that the vertical structure of the *ztend*2 change is related to that of the change of mean vertical divergence in the troposphere. We further analyze vertical profiles of vertical velocity (Fig. 4). Radiative cooling is suppressed from NCR to CTL in the upper troposphere and the lower troposphere (Fig. 1), which leads to the weakened upward motions from the upper troposphere to the lower troposphere (Fig. 4). As a result, less vertical mass convergence occurs from NCR to CTL (Fig. 3), which causes the increase in *ztend*2 from NCR to CTL. Since the difference between CTL and NCR is those in the cloud radiative processes, the reduced radiative cooling in the upper troposphere is larger than

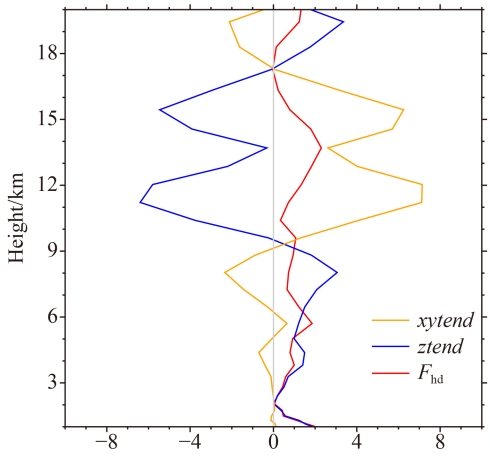

Fig. 2 Vertical profiles of differences in the heat flux divergence (F_{hd}; red) and its components: divergence of horizontal heat flux (*xytend*; orange) and divergence of vertical heat flux (*ztend*; blue) between the control experiment and the sensitivity experiment. Unit is °C·d^{-1}.

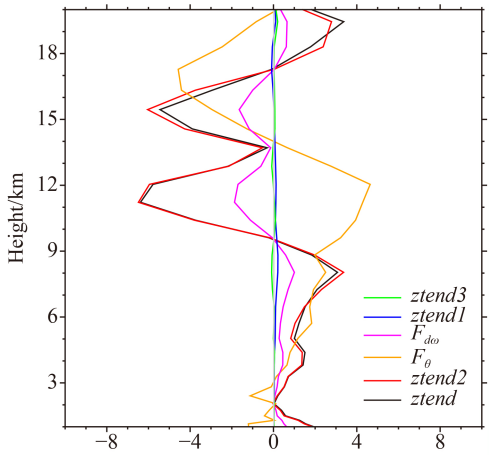

Fig. 3 Vertical profiles of differences in vertical heat flux divergence (*ztend*; black; °C·d^{-1}), interaction between mean temperature and mean vertical divergence (*ztend*2; red; °C·d^{-1}), mean temperature (F_θ; orange; 10^{-1} °C), vertical divergence ($F_{d\omega}$; magenta; 10^{-2} d^{-1}), mean vertical temperature advection (*ztend*1; blue; 10^{-1} °C·d^{-1}), the divergence of perturbation vertical heat flux (*ztend*3; green; °C·d^{-1}) between the control experiment and the sensitivity experiment.

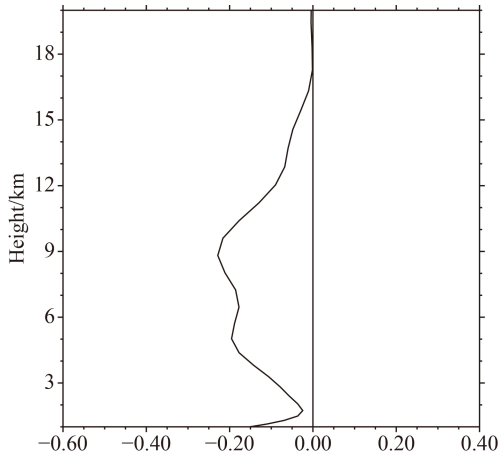

Fig. 4 Vertical profiles of differences in $-\omega$ ($\sim w$;10^{-3} Pas^{-1}) between the control and sensitivity experiments.

Table 3 Daily and model domain means of surface rain rate (P_S), net condensation (Q_{NC}), and hydrometeor convergence/divergence (Q_{CM}) for (a) convective rainfall and (b) stratiform rainfall in CTL, and NCR, and their differences (CTL−NCR)

Convective rainfall			
(a)	CTL	NCR	CTL−NCR
P_S	52.330	55.430	−3.100
Q_{NC}	64.480	68.930	−4.450
Q_{CM}	−12.160	−13.470	1.310

Stratiform rainfall			
(b)	CTL	NCR	CTL−NCR
P_S	17.220	17.280	−0.06
Q_{NC}	5.230	4.700	0.53
Q_{CM}	11.990	12.580	−0.59

that in the lower troposphere (Fig. 1), which leads to stability in the troposphere. Thus, the suppressed instability from NCR to CTL in the troposphere (Fig. 4) is associated with suppressed radiative cooling (Fig. 1).

In total, although the enhanced radiative cooling from the sensitivity experiment to the control experiment occurs above 11 km and the weakened radiative cooling from the sensitivity experiment to the control experiment appears below 11 km (Fig. 1), the tropopause usually is about 10–11 km where the radiative cooling is similar in both the control experiment and the sensitivity experiment. Consequently, the weakened radiative cooling from the sensitivity experiment to the control experiment appears in the troposphere, resulting in reduced upward motions from the sensitivity experiment to the control experiment (Fig. 4).

To investigate the cloud radiation effects on convective and stratiform rainfall, we further separate the surface rainfall into convective and stratiform rainfall components. Table 3 shows the temporally-spatially averaged rainfall budget in CTL and NCR and their difference. It shows that the reduced rainfall from NCR to CTL is mainly associated with the reduced convective rainfall. The reduced convective rainfall is about one magnitude larger than the stratiform rainfall. Namely, time-mean stratiform rainfall is not sensitive to cloud radiative processes. The reasons could be as follows: stratiform rainfall is only associated with ice clouds, where the radiative cooling is suppressed as height increases from 6 km to 8 km but enhanced as height increases from 8 km to 11 km. Furthermore, the reduced convective rainfall is mainly connected to the decreased net condensation over the convective rainfall area (Table 3(a)).

To examine the cloud radiation effects on convective and stratiform rainfall in more detail, Fig. 5 further shows the temporal variations of spatially averaged rainfall budgets in CTL and NCR and their differences. It shows that the reduced rainfall from NCR to CTL is mainly associated with reduced convective rainfall during the daytime, while stratiform rainfall plays a minor role. During the day time, stratiform rainfall decreases from NCR to CTL, but it occasionally increases (Figs. 5(a)–5(c)). Stratiform rainfall mainly reduces from NCR to CTL during the daytime, occasionally increasing. Therefore, the difference in stratiform rainfall is negligibly smaller than that in convective rainfall in area-mean analysis. Reduced stratiform rainfall from NCR to CTL is primarily associated with decreased hydrometeor convergence, whereas increased stratiform rainfall is primarily associated with increased net condensation (Figs. 5(d)–5(f)).

We also attempt to know if the explanation of cloud radiative effects on temporally-spatially averaged rainfall can be applied to the explanation of cloud radiative effects on temporal variation of spatially averaged rainfall since cloud radiative effects may differ from daytime to nighttime. Considering cloud solar radiative and infrared radiative effects on rainfall may be different. Figure 6 shows that solar radiation is heating the whole troposphere, decreasing the top infrared cooling and reducing base warming, which leads to the stability of the troposphere (Figs. 6(a)–6(c)), while the infrared radiation increases top cooling and base warming, which leads to a destabilizing effect on the troposphere (Figs. 6(d)–6(f)). The solar radiation effects are more important than infrared radiation during the daytime, leading to the more stabilized troposphere and weaker upward motions (Figs. 7 and 8) due to less rainfall during the daytime in the control simulation compared to the NCR simulation. Infrared radiation is dominant during the nighttime (generally 1000–1600 UTC), leading to a more unstabilized troposphere and stronger upward motions (Figs. 7 and 8) due to more rainfall during the nighttime in the control simulation compared to the NCR simulation.

Cloud radiative effects on temporally-spatially averaged rainfall are suppressed from NCR to CTL during the peak of rainfall. Namely, more radiative

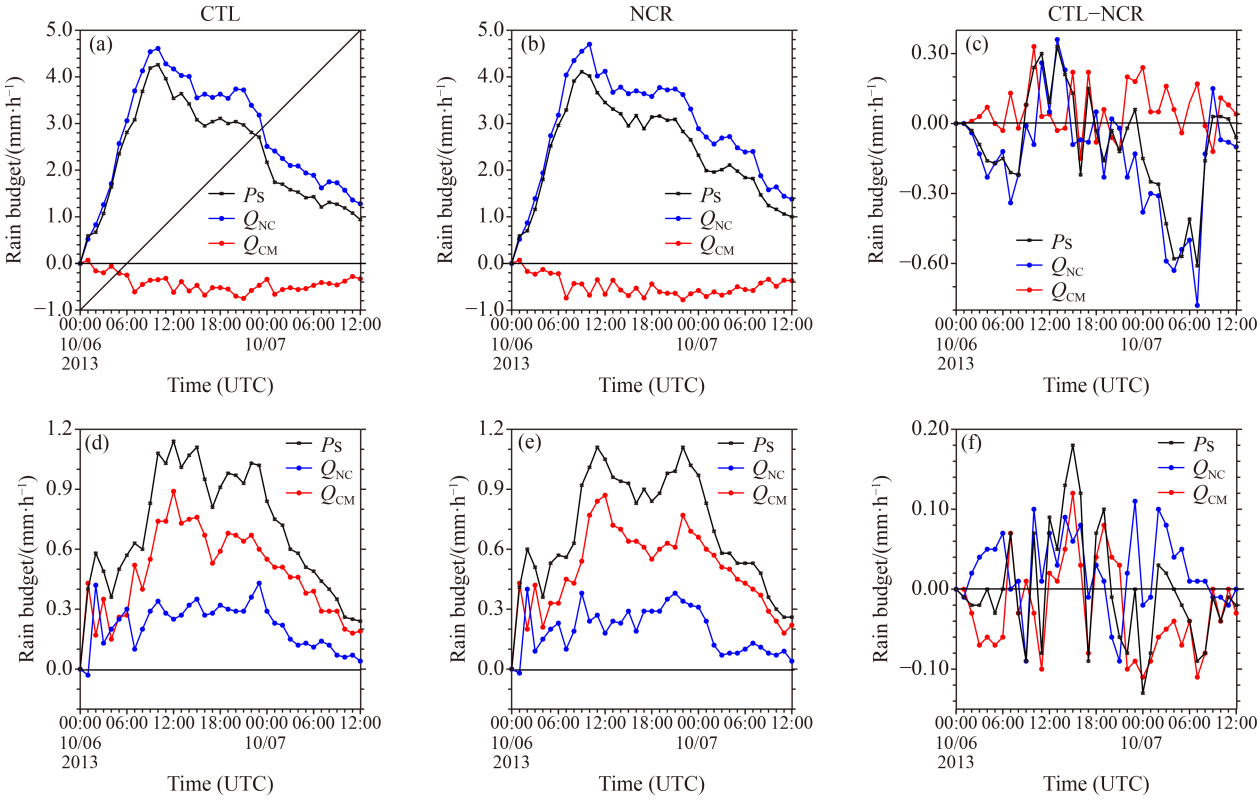

Fig. 5 Time series of domain-mean surface rain rate (P_S), net condensation (Q_{NC}), and hydrometeor convergence/divergence (Q_{CM}) for (a–c) convective rainfall and (d–f) stratiform rainfall in (a, d) CTL, and (b, e) NCR, and (c, f) their differences (CTL−NCR).

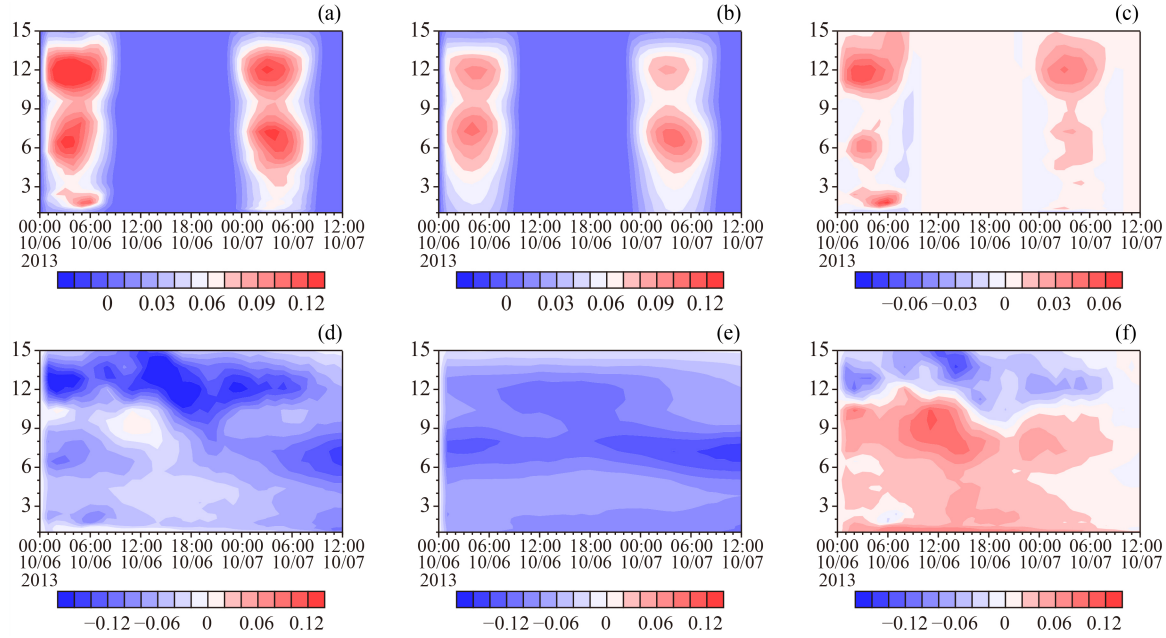

Fig. 6 The temporal-vertical cross-section of (a, d) control, (b, e) NCR, and (c, f) their difference (CTL−NCR) in (a, b, c) solar radiative heating and (d, e, f) infrared radiative cooling between CTL to NCR. Unit: K·h^{-1}.

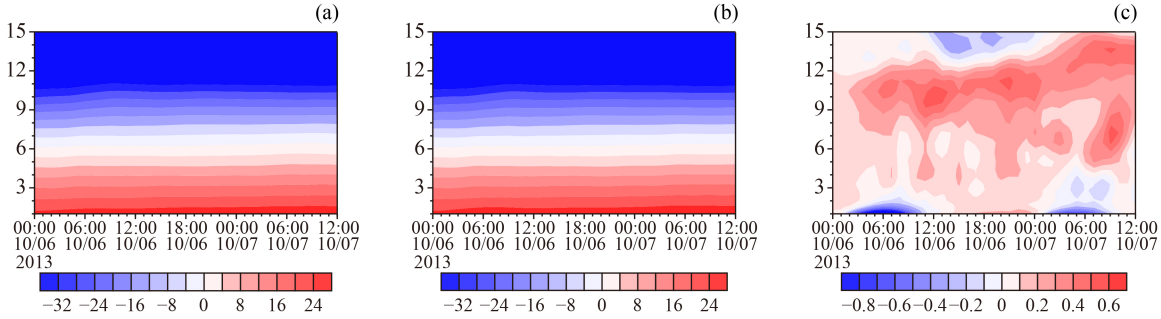

Fig. 7 The temporal-vertical cross-section of (a) control, (b) NCR, and (c) their difference (CTL−NCR) in temperature (unit: °C) between CTL to NCR.

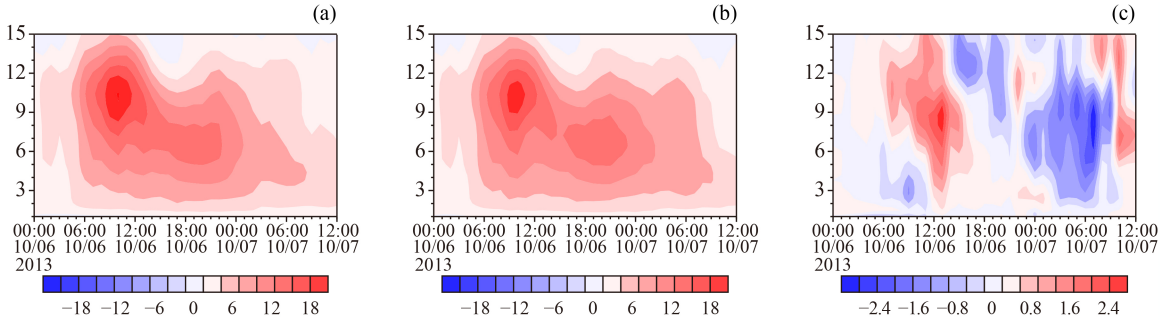

Fig. 8 The temporal-vertical cross-section of (a) control, (b) NCR, and (c) their difference (CTL−NCR) in vertical velocity (~w; cm·s^{-1}) between CTL to NCR.

cooling due to the exclusion of cloud radiative effects causes stronger rainfall in NCR than in control, consistent with previous results about the effects of IR cooling on convection (e.g., Li et al., 1999; Tao et al., 1996).

4 Summary

Sensitivity experiments on Typhoon Fitow (2013) were conducted with the three-dimensional WRF model to examine cloud-radiation feedbacks on heat budget and surface precipitation during its landfall. The simulation data were used to analyze the difference in heat budget between the experiments including and excluding cloud radiative effects. The analysis shows that the decrease in the heat flux divergence from the experiment removing cloud radiative effects to the control experiment has a similar magnitude and vertical profile to the reduction in radiative cooling.

The inclusion of radiative effects of clouds reduces radiative cooling via reducing outgoing radiation. The enhanced radiative cooling decreases from the upper troposphere to the lower troposphere. The decreased instability increases from the mid-troposphere to the lower troposphere, reducing vertical mass convergence. The weakened mass convergence leads to a reduction in the vertical heat flux divergence that increases air temperature and saturation mixing ratio. As a result, net condensation and the associated latent heat release are reduced, and the rainfall is decreased.

The rainfall was further partitioned into convective rainfall and stratiform rainfall. The cloud radiation effects on convective and stratiform rainfall were further analyzed. The inclusion of clouds radiation effects results in decreased rainfall. The decreased rainfall is associated with reduced convective and stratiform rainfall. Both convective and stratiform rainfall in the nighttime increased due to the increased net condensation and hydrometeor convergence, respectively. The decreased convective rainfall is related to the reduced net condensation in the daytime, while the decreased stratiform rainfall is associated with the reduced hydrometeor convergence in the daytime.

In summary, the inclusion of cloud radiative effects reduced latent heat release due to constraints on surface rainfall. Further partitioning rainfall into convective and stratiform components shows different processes affecting convective and stratiform rainfall. Decreased surface rainfall is mainly associated with decreased convective and stratiform rainfall. However, the constraint on convective rainfall is associated with a decrease in net condensation, while the constraint on stratiform rainfall is associated with a decreasing hydrometeor convergence (Fig. 9).

Caution should be exercised when the results are applied since the results are based on the case study of Typhoon Fitow in 2013. Further examination of more cases should be conducted to validate and generalize the results from this study.

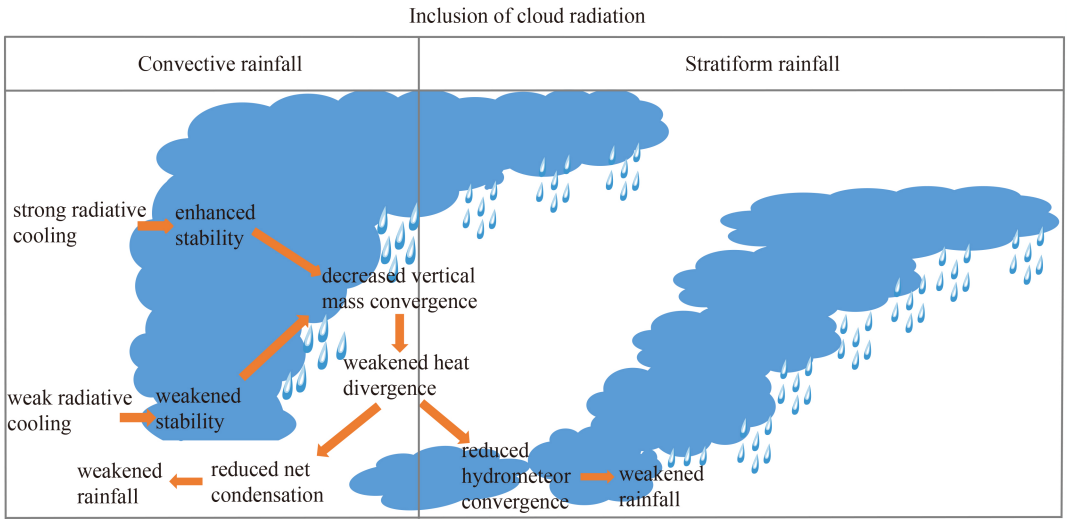

Fig. 9 A conceptual model for the probable mechanism of cloud radiation process affects precipitation.

Acknowledgments We thank the three anonymous reviewers for their suggestive comments, which greatly help us improve the quality of the manuscript. The best track data may be obtained from WZTF121 website. The NCEP FNL data with 1° × 1° horizontal resolution was obtained from the NCAR UCAR Research Data Archive Computational and Information System Laboratory (available at NCAR UCAR website). All data are archived at the Training Center of Atmospheric Sciences of Zhejiang University and are also available from the authors via xuhuiyan8888@163.com. The authors gratefully acknowledge the assistance of the Training Center of Atmospheric Sciences of Zhejiang University. This work was supported by the Natural Science Foundation of Zhejiang Province of China (No. LQ20D050001), and National Natural Science Foundation of China (Grant No. 42105004), and the Scientific Research Foundation of Hangzhou Normal University (No. 2020QDL015).

References

Braun S A, Montgomery M T, Mallen K J, Reasor P D (2010). Simulation and interpretation of the genesis of Tropical Storm Gert (2005) as part of the NASA tropical cloud systems and processes experiment. J Atmos Sci, 67(4): 999–1025

Cecelski S F, Zhang D (2016). Genesis of Hurricane Julia (2010) within an African easterly wave: sensitivity to ice microphysics. J Appl Meteorol Climatol, 55(1): 79–92

Chen L, Li Y, Cheng Z (2010). An overview of research and forecasting on rainfall associated with landfalling tropical cyclones. Adv Atmos Sci, 27(5): 967–976

Dudhia J (1989). Numerical study of convection observed during the winter monsoon experiment using a mesoscale two-dimensional model. J Atmos Sci, 46(20): 3077–3107

Dudhia J (1996). A multi-layer soil temperature model for MM5. Sixth Annual PSU/NCAR Mesoscale Model Users' Workshop. Boulder: Colorado: 22–24

Feng Z, Dong X, Xi B, Schumacher C, Minnis P, Khaiyer M (2011). Top-of-atmosphere radiation budget of convective core/stratiform rain and anvil clouds from deep convective systems. J Geophys Res, 116(D23): D23202

Fu Q, Krueger S K, Liou K N (1995). Interactions of radiation and convection in simulated tropical cloud clusters. J Atmos Sci, 52(9): 1310–1328

Gao S, Cui X P, Li X (2009). A modeling study of diurnal rainfall variations during the 21-day period of TOGA COARE. Adv Atmos Sci, 26(5): 895–905

Gao S, Li X (2010). Precipitation equations and their applications to the analysis of diurnal variation of tropical oceanic rainfall. J Geophys Res, 115(D8): D08204

Gray W M, Jacobson R W Jr (1977). Diurnal variation of deep cumulus convection. Mon Weather Rev, 105(9): 1171–1188

Houze R A Jr (1997). Stratiform precipitation in regions of convection: a meteorological paradox? Bull Am Meteorol Soc, 78(10): 2179–2196

Li X, Gao S (2011). Precipitation Modeling and Quantitative Analysis. Dordrecht: Springer Science & Business Media

Li X, Sui C H, Lau K M, Chou M D (1999). Large-scale forcing and cloud-radiation interaction in the tropical deep convective regime. J Atmos Sci, 56(17): 3028–3042

Li X, Zhai G, Gao S, Shen X (2014). A new convective–stratiform rainfall separation scheme. Atmos Sci Lett, 15: 245–251

Lilly D K (1988). Cirrus outflow dynamics. J Atmos Sci, 45(10): 1594–1605

Lin Y, Farley R D, Orville H D (1983). Bulk parameterization of the snow field in a cloud model. J Clim Appl Meteorol, 22(6): 1065–1092

Mlawer E J, Taubman S J, Brown P D, Iacono M J, Clough S A (1997). Radiative transfer for inhomogeneous atmospheres: RRTM, a validated correlated-k model for the longwave. J Geophys Res, 102(D14): 16663–16682

Shen X, Wang Y, Li X (2011a). Effects of vertical wind shear and cloud radiative processes on responses of rainfall to the large-scale forcing during pre-summer heavy rainfall over southern China. Q J R Meteorol Soc, 137(654): 236–249

Shen X, Wang Y, Li X (2011b). Radiative effects of water clouds on rainfall responses to the large-scale forcing during pre-summer heavy rainfall over southern China. Atmos Res, 99(1): 120–128

Shen X, Wang Y, Zhang N, Li X (2010). Roles of large-scale forcing, thermodynamics, and cloud microphysics in tropical precipitation

processes. Atmos Res, 97(3): 371–384

Shu S, Xu H, and Zhang W (2020). Convective-stratiform rainfall of Typhoon Fitow (2013): sensitivity to rainfall partitioning methods. J Geophys Res Atmos, 125: e2019JD031510

Skamarock W C, Klemp J B, Dudhia J, Gill D O, Barker D M, Duda M G, Huang X, Wang W, Powers J G (2008). A description of the Advanced Research WRF version 3, NCAR Tech, Note NCAR/TN-475+STR

Steiner M, Houze R A Jr (1993). Three-dimensional validation at TRMM ground truth sites: some early results from Darwin, Australia. In: 26th Int. Conf. on Radar Meteorology, Norman, OK, Amer Meteor Soc, 417–420

Sui C H, Lau K M, Takayabu Y N, Short D A (1997). Diurnal variations in tropical oceanic cumulus convection during TOGA COARE. J Atmos Sci, 54(5): 639–655

Sui C H, Lau K M, Tao W K, Simpson J (1994). The tropical water and energy cycles in a cumulus ensemble model. Part I: equilibrium climate. J Atmos Sci, 51(5): 711–728

Sui C H, Li X, Lau K M (1998). Radiative-convective processes in simulated diurnal variations of tropical oceanic convection. J Atmos Sci, 55(13): 2345–2357

Sui C H, Tsay C T, Li X (2007). Convective-strati_form rainfall separation by cloud content. J Geophys Res, 112(D14): D14213

Tao W K, Lang S, Simpson J, Sui C H, Ferrier B, Chou M D (1996). Mechanisms of cloud-radiation interaction in the tropics and midlatitudes. J Atmos Sci, 53(18): 2624–2651

Wang B, Xu H, Zhai G, Li X (2018). The rainfall responses of Typhoon Soudelor (2015) to radiative processes of cloud species. J Geophys Res Atmos, 123(8): 4284–4293

Wang D, Li X, Tao W K (2010a). Cloud radiative effects on responses of rainfall to large-scale forcing during a landfall of severe tropical storm Bilis (2006). Atmos Res, 98(2–4): 512–525

Wang D, Li X, Tao W K (2010b). Torrential rainfall responses to radiative and microphysical processes of ice clouds during a landfall of severe tropical storm Bilis (2006). Meteorol Atmos Phys, 109(3–4): 107–114

Xu H, Li X (2017). Torrential rainfall processes associated with a landfall of typhoon Fitow (2013): a three-dimensional WRF modeling study. J Geophys Res, 122(11): 6004–6024

Xu K, Randall D A (1995a). Impact of interactive radiative transfer on the macroscopic behavior of cumulus ensembles. Part I: radiation parameterization and sensitivity tests. J Atmos Sci, 52(7): 785–799

Xu K, Randall D A (1995b). Impact of interactive radiative transfer on the macroscopic behavior of cumulus ensembles. Part II: mechanisms for cloud-radiation interactions. J Atmos Sci, 52(7): 800–817

Yin J, Wang D, Zhai G, Wang H, Xu H, Liu C (2022). A modified double-moment bulk microphysics scheme toward the East Asia Monsoon region. Adv Atmos Sci

Yu Z (2014). Overview of Severe Typhoon Fitow and its Operational Forecasts. Trop Cyclone Res Rev, 3: 22–34

Zhu H, Xu H, Li X (2018). Thermal and microphysical effects of ice clouds on torrential rainfall over northern China. J Geophys Res Atmos, 123(21): 12228–12235